CRYSTAL ORIENTATION DEPENDENT ETCHING IN RIE AND ITS APPLICATION

S. Tanaka[1], K. Sonoda[1,2], K. Kasai[2], K. Kanda[1,2], T. Fujita[1,2], K. Higuchi[2], and K. Maenaka[1,2]
[1]Department of Electrical Engineering and Computer Science, Graduate School of Engineering, University of Hyogo, Shosha 2167, Himeji, Hyogo, Japan
[2]Maenaka Human-Sensing Fusion Project, JST, shosha 2167, Himeji, Hyogo, Japan

ABSTRACT

We found that an appropriate mixture of SF_6, C_4F_8 and O_2 gases in a standard Inductively Coupled Plasma Reactive Ion Etching (ICP-RIE) apparatus achieves crystal orientation dependent etching. The etched shapes after the RIE of silicon wafers with (100), (110), and (111) surface orientation are investigated by the masks with circular openings and isolated pattern. The results of the etching process show (111) terraces; i.e., the etching rate of the (111) plane is slower than that of other planes similar to the alkaline-based wet etching. The etching rate in the horizontal direction in each crystallographic orientation is examined by etching a wagon wheel pattern. We also demonstrate an application, Through-Silicon Via (TSV) holes with horn-shaped openings using this process.

INTRODUCTION

Anisotropic wet etching has been widely used as a basic silicon micromachining process. In dry etching, a commercial Deep Reactive Ion Etching (DRIE) apparatus that uses the Bosch process can achieve vertical anisotropic etching of silicon. The Bosch process uses cyclic switching between SF_6-based etching and C_4F_8-based passivation. DRIE of silicon has also found many applications in bulk micromachining. A crystal anisotropic dry etching by special process condition or apparatus has also been reported, for instance, a chlorine-based plasma etching [1] or SF_6 cryogenic etching with extremely low substrate temperatures ($< -80°C$) [2][3]. We reported that an appropriate mixture of SF_6, C_4F_8, and O_2 gases in a standard ICP-RIE apparatus achieves crystal orientation dependent etching [4]. Simultaneously, Mishima et al reported that mixture of SF_6 and C_2F_6 gases in RIE also achieves crystalline anisotropic etching [5]. These processes are very simple and comfortable for MEMS fabrication because a common photoresist can be used as the masking material contrary to the alkaline etching.

In this paper, we examine the details of the anisotropic etching in RIE. The etched shapes after crystal anisotropic etching of silicon wafer for the masks with circular openings and isolated pattern are investigated. In addition, the variation in etched shapes with the time and size of the mask opening are also examined. To obtain detailed data on the crystal orientation dependence of the etching rates, a wagon wheel shaped masking pattern [6] is employed. Our process features a higher etching rate in the <111> crystal orientation than wet etching, although the rate is slower than that for the other planes. At unmasked region, the etching rate in the vertical direction is faster than that in the lateral direction because the unmasked portion of the surface is exposed to etching plasma with a high kinetic energy. Thus, even if the silicon wafer has (111) surface orientation, we can perform the vertical etching for unmasked region with considerably high etching rate. This feature is completely different from alkaline wet etching.

We also demonstrate an application, TSV with horn-shaped openings using the etching technology presented here.

EXPERIMENTS AND RESULTS

We examine the details of anisotropic etching using a mixture of SF_6, C_4F_8, and O_2 gases in a commercial ICP-RIE apparatus (Pegasus®; Sumitomo Precision Products, Japan). The process recipe is within a normal operating range (coil power 1200 W, platen power 25 W, pressure 10 Pa, substrate temperature 10°C) and SF_6 (160 sccm), C_4F_8 (120 sccm), and O_2 (200 sccm) gases are continuously applied (non-Bosch process). In the experiments, 4-inch silicon wafers with (100) (p-type), (110) and (111) (n-type) surface orientation are used.

Mask with circular openings

Circular mask openings with a diameter of 60 μm are prepared as shown in Fig. 1 (a). After etching for 50 minutes, the etched shapes are observed. Figure 1 (b) shows a top view of a (100) wafer with the photo resist mask, where the dark center patterns are the mask openings, and the shadowy areas around the openings are undercut etching. Figures 2 (a), (c), and (e) show top views of (100), (110), and (111) wafers and Figs. 2 (b), (d), and (f) show the cross sections along the A-A' lines in Figs. 2 (a), (c), and (e). These Scanning Electron Microscope (SEM) photographs clearly show the crystal orientation dependent etching. Figures 2 (b), (d), and (f) also show the reference lines for the theoretical inclination angle of the (111) walls, which are 54.7°, 90.0°, and 70.5°, respectively. Figure 3 shows the measured vertical etching rates at the unmasked portion for the (100), (110), and (111) silicon wafer versus the size of the mask opening, where the etching rate of the (111) planes is slightly slower than that of the other planes. Figures 4 (a), (c), and (e) show the cross-sectional shape with etching time as a parameter for (100), (110), and (111) wafers. The etching durations are 10, 20, 30, 40, and 50 minutes and the size of the mask opening is 100 μm. Figures 4 (b), (d), and (f) show the cross-sectional shape versus the size of the mask openings on (100), (110), and (111) wafers. The sizes of the mask opening are 20, 40,

60, 80, and 100 µm and the etching duration is 50 minutes.

Our etching process achieves (111) terraces; i.e., the etching rate of the (111) plane is slower than that of the other planes, similar to alkaline-based wet etching. Figures 4 (a), (c), and (e) show that the etching rate in the vertical direction is faster than that in the lateral direction regardless of orientation; this is because the unmasked portion of the surface is exposed to etching plasma with a high kinetic energy. Thus, the unmasked silicon surface is etched for any surface orientation. As a result, two regions appear: the bottom surface obtained from vertical etching, and the lateral undercut etching spread from sidewall of the vertical etching. Figures 4 (b), (d), and (f) show that the etching rate decreases as the size of mask opening reduces, which is because of the microloading effect.

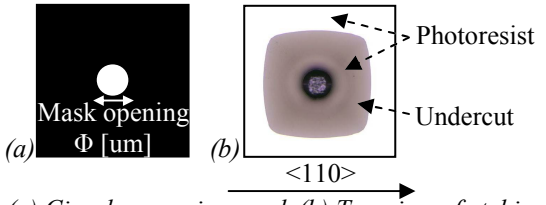

Figure 1: (a) Circular opening mask (b) Top view of etching results for (100) wafer with circular opening mask in Fig.1 (a). Undercut etching is visible.

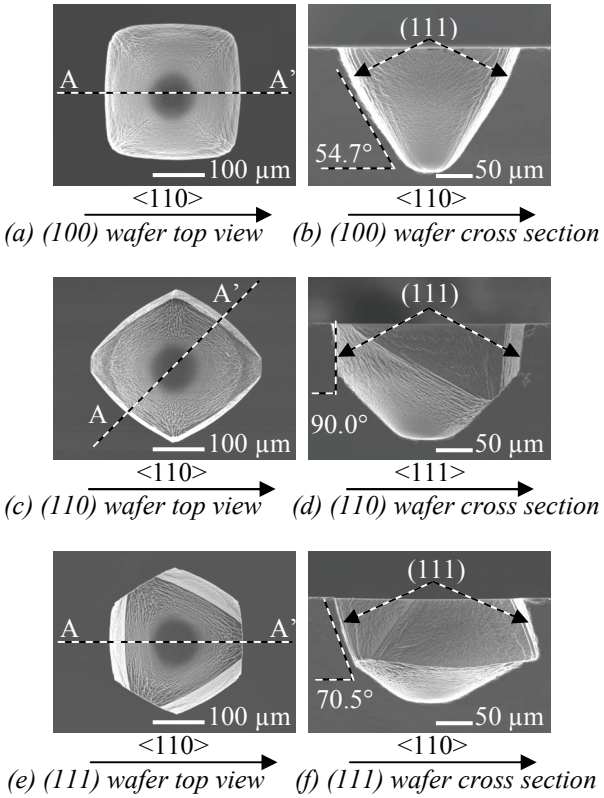

Figure 2: Top surface and cross-sectional SEM images of etching results for Si wafers with circular opening mask.

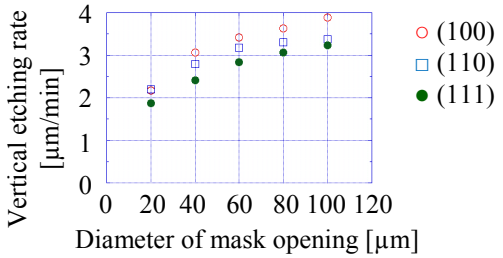

Figure 3: Vertical etching rate vs. diameter of mask opening for (100), (110), and (111) wafers.

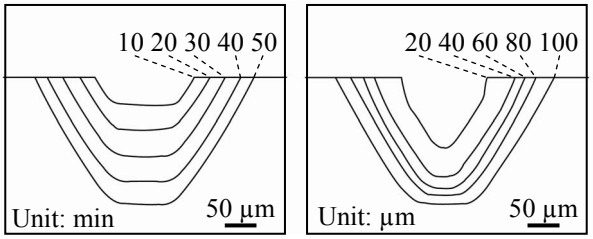

(a, left) Cross-sectional shape vs. etching time on (100) wafer. (b, right) Cross-sectional shape vs. mask opening on (100) wafer.

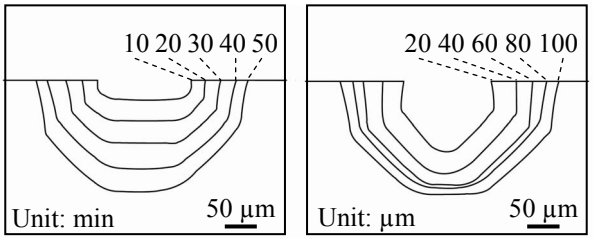

(c, left) Cross-sectional shape vs. etching time on (110) wafer. (d, right) Cross-sectional shape vs. mask opening on (110) wafer.

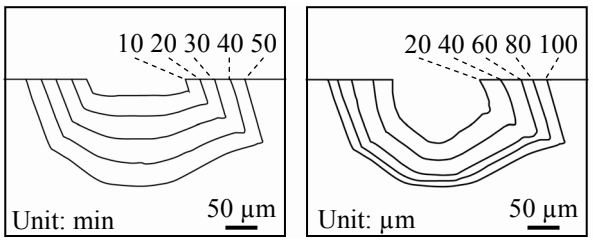

(e, left) Cross-sectional shape vs. etching time on (111) wafer. (f, right) Cross-sectional shape vs. mask opening on (111) wafer.

Figure 4: Variation in etched shapes with time and various sizes of mask opening. All shapes were obtained from SEM images.

Isolated pattern

By the mask pattern as shown in *Fig.* 5, an isolated island structure was formed. In the experiments, a p-type

silicon wafer with (100) surface orientation is used. The diameter of the circular pattern is 200 µm. Figures 6 (a) and (b) show the top views of the wafer after etching for 20 and 60 minutes, respectively. In Fig. 6 (b), a pyramidal-shaped silicon pattern remains. As the etching advances, the crystal surface with slow etching rate disappears and surface with fast etching rate appears. From Fig. 6 (b), we can find that (100) or (110) surfaces have high etching rate rather than other surfaces.

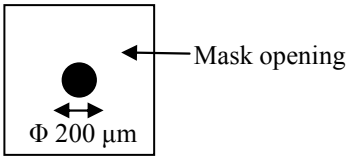

Figure 5: Circular isolated pattern in square shape opening mask.

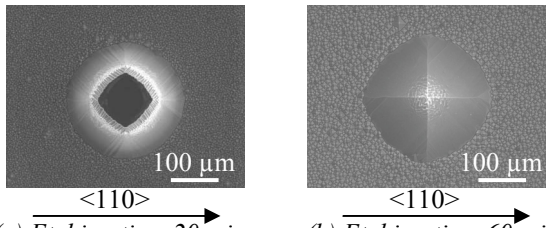

(a) Etching time 20 min. *(b) Etching time 60 min.*

Figure 6: Circular isolated pattern after etching of (100) wafer. Top surface SEM images.

Wagon wheel pattern

To obtain detailed data on the crystal orientation dependence of the etching rate, the wagon wheel shaped masking pattern in Fig. 7 is employed. The pattern consists of rectangular radial segments that are 50 µm × 10 mm in size. First, photoresist is spin-coated over a 1-µm-thick thermal oxide covering on the wafer. Then, the oxide and photoresist layers are patterned to make an etching mask. After etching for 40 minutes, the etched shapes are observed. To obtain quantitative results, the lateral etching rates are determined by measuring the width *w* of the side etching under the masking layer. The schematic cross section of the wagon wheel pattern after etching is illustrated in Fig. 8. Figures 9 (a), (c), and (e) show the etched pattern for the wafers with (100), (110), and (111) surface orientation. The figures show a dark pattern that extends radially from the center. This phenomenon is caused by the connection of the rectangular segments to the adjoining segments due to the undercut etching. The lateral under-etching rates of these planes on (100), (110), and (111) wafers are shown in the polar coordinate diagrams in Figs. 9 (b), (d), and (f). The obtained etching shape is somewhat different from usual anisotropic wet etching; this is because the ratio of etching rate (100)/(111) or (110)/(111) is not so high. The etching shape is a result of combination of the vertical etching (usual RIE) and side etching with crystal anisotropy. Thus conventional analysis method cannot directly be used. We are now trying to establish complete discussion for anisotropy in our process.

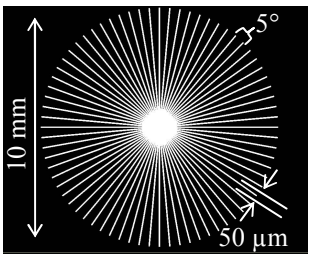

Figure 7: Wagon wheel pattern.

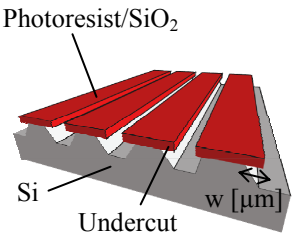

Figure 8: Schematic cross section of wagon wheel pattern after etching.

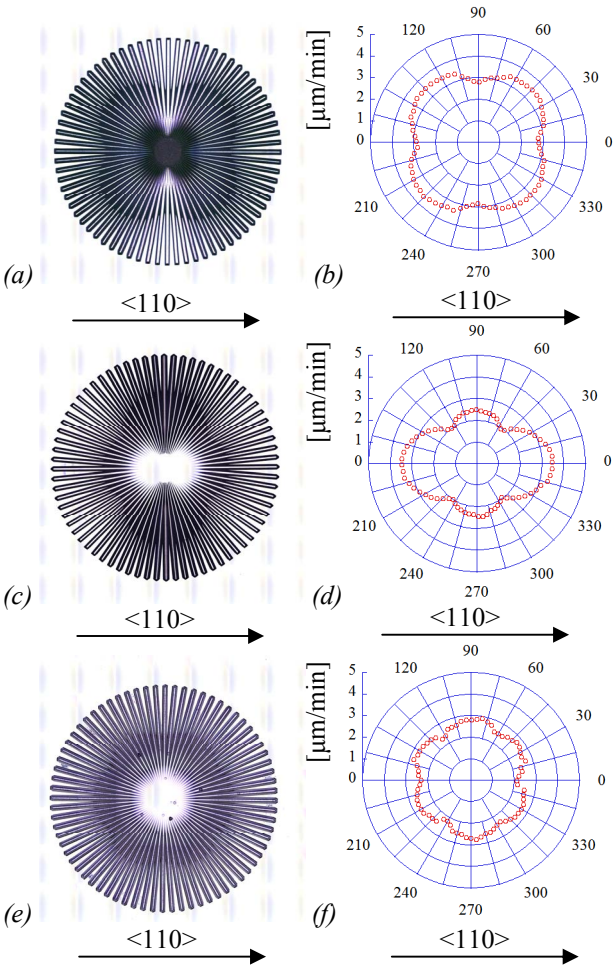

Figure 9: (a), (c), (e) Etch patterns in (100), (110), and (111) surface orientations. (b), (d), (f) Lateral under-etching rates in (100), (110), and (111) surface orientations.

APPLICATION TO TSV

The anisotropic RIE process is useful for realization of a controlling the shape of via holes or cavity structures. For examples, a combination of dry deep trench etching followed by a crystallographic anisotropic wet etching is sometimes used to define the shape of the trench [7]. Using our technique, these structures can be achieved only by changing the recipe of the dry etching. There is no need to apply a wet

etching process and additional process steps to protect devices against the alkaline solution. In this paper, we demonstrate an application, TSV holes with horn-shaped openings. Such openings are useful for conformal deposition of insulator and metallic layers, for easy lithography in the holes and for burying solder balls in the wafer-level packaging [8].

Figure 10 shows the fabrication process. First, photoresist is spin-coated on a (100) wafer (Fig.10 (a)), and the photoresist is patterned in circular mask openings (Fig. 10 (b)). Next, the wafer is etched by crystallographic anisotropic etching (Fig. 10 (c)). The backside of the wafer is etched as the same manner (Fig. 10 (d)). Then, the wafer is etched by a DRIE penetration etching process (Bosch process) (Fig. 10 (e)). Finally, the photoresist mask is removed from the wafer. The total process is very simple because a photoresist can be used for the masking material contrary to use of the alkaline etchant. The shape of the edge of the hole is of course defined by the crystal orientation. Figure 11 shows a cross section of the through hole produced by crystallographic anisotropic etching and the Bosch process. Figure 12 shows the TSV holes with copper as a filler material. After TSV etching, a 1-µm-thick thermally oxidized film is grown and both side sputtering layer of a Au/Cr (5 µm) metal is deposited as a seed layer followed by electroplating of copper.

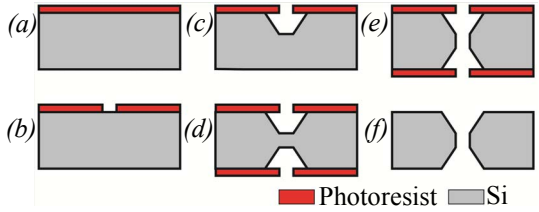

Figure 10: Through hole process flow.

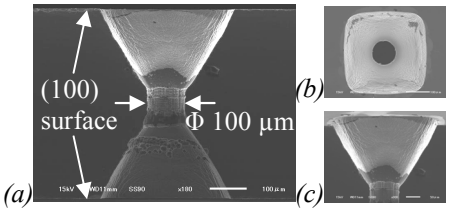

Figure 11: Application of presented technology to silicon via holes. (a) Cross section, (b) top view of opening, (c) close-up of quadrangular pyramidal horn.

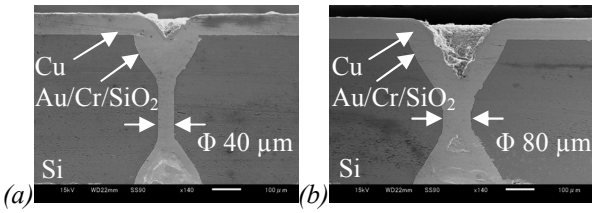

Figure 12: Copper plating for TSV. (a) Mask opening 40 µm in diameter. (b) Mask opening 80 µm in diameter.

CONCLUSIONS

An appropriate mixture of SF_6, C_4F_8, and O_2 gases in a standard ICP-RIE apparatus achieves crystal orientation dependent etching. The features of the crystal anisotropy etching in RIE are similar to those of anisotropic wet etching. The etching rate in the (111) crystal orientation is slower than that in the (100) and (111) orientations. When the mask with circular openings is used, the crystal face with a slow etching rate determines the shape after etching. In case of the mask with isolated patterns, the crystal face with a fast etching rate determines the shape after etching. These results are similar to alkaline-based wet etching. However, the etching rate in the vertical direction is faster than that in the lateral direction regardless of the crystal orientation; this is because the unmasked portion of the surface is exposed to etching plasma with a high kinetic energy. We also found the etching rate is slightly slowed by the microloading effect when the size of the mask decreases. The etching rate in the lateral direction in each crystallographic orientation was examined by etching a wagon wheel pattern. Additionally, we are utilizing this process technology for fabrication of TSV holes with horn-shaped openings. The horn-shaped opening is expected to be useful for conformal deposition of an insulator and metallic layers and also for burying solder balls in the wafer-level packaging.

REFERENCES

[1] H. Kinoshita and K. Jinno, "Anisotropic Etching of Silicon by Gas Plasma", Jpn. J. Appl. Phys., vol. 16, pp. 381-382, 1977.

[2] L. Sainiemi, "Cryogenic Deep Reactive Ion Etching of Silicon Micro and Nanostructures", Doctoral Dissertation, Helsinki Univ. of Tech., 2009.

[3] M. A. Blauw, "Deep Anisotropic Dry Etching of Silicon Microstructures by High-Density Plasmas", PhD thesis, Delft Univ. of Tech., 2004.

[4] S. Tanaka, K. Maenaka, K. Sonoda, K. Kanda, T. Fujita, K. Kasai, and K. Higuchi, "Crystallographic Anisotropic Etching in RIE and Its Application to Through Silicon Via", Book of Abstracts, The 27th Sensor Symposium on Sensors, Micromachines and Applied Systems, p. 119, 2010.

[5] T. Mishima, K. Terao, H. Takao, F. Shimokawa, F. Oohira, and T. Suzuki, "Crystalline Anisotropic Etching for Single Crystal Silicon Using Dry Etching", Book of Abstracts, The 27th Sensor Symposium on Sensors, Micromachines and Applied Systems, p. 118, 2010.

[6] H. Seidel, L. Csepregi, A. Heuberger and H. Baumegärtel, "Anisotropic Etching of Crystalline Silicon in Alkaline Solutions", J. Electrochem. Soc., vol. 137, pp. 3612-3626, 1990.

[7] Y. Li, M. Sasaki, and K. Hane, "Fabrication and Testing of Solid Polymer Dye Microcavity Lasers Based on PMMA Micromolding", J. Micromech. Microeng., vol. 11, pp. 234-238, 2001.

[8] M. Esashi, "Wafer Level Packaging of MEMS", J. Micromech. Microeng., vol. 18, pp. 1-13, 2008.